TSINGHUA SCIENCE AND TECHNOLOGY
ISSN 1007-0214 12/19 pp688-693
Volume 9, Number 6, December 2004

Valveless Thermally-Driven Phase-Change Micropump*

WANG Moran(王沫然), LI Zhixin(李志信)**

Department of Engineering Mechanics, Tsinghua University, Beijing 100084, China

Abstract: A dynamic model with moving heat sources was developed to analyze the pumping mechanism of a valveless thermally-driven phase-change micropump. The coupled equations were solved to determine the pumping characteristics. The numerical results agree with experimental data from micropumps with different diameter microtubes. The maximum flow rate reached 33 μL / min and the maximum pump pressure was over 20 kPa for a 200-μm diameter microtube. Analysis of the pumping mechanism shows that the main factors affecting the flow come from the large density difference between the liquid and vapor phases and the choking effect of the vapor region.

Key words: valveless; micropump; phase change; pumping mechanism

Introduction

Micropumps are important actuators in microfluidic systems. With the rapid development of micro-electro-mechanical system(MEMS) technologies, mechanical micropumps can be fabricated much smaller. However, the pump size and the characteristics are still limited by the manufacturing. During recent years, different valveless micropumps have been proposed using fluid property changes, including even phase changes, instead of valves with movable parts[1-5]. Valveless micropumps reduce the valve failure risk and usually simplify the fabrication process.

Fluids in microchannels can change phases quickly due to the decreased thermal inertia. Therefore, phase change can be easily applied to micro actuators[4-6]. The idea of using vapor-liquid phase change in a channel to pump fluid was first mentioned to 1992[7]. The pumping principle of the first phase-change micropump was similar to that of a thermopneumatic pump. The phase-change fluid was heated by a laser and separated from the working fluid, but this led to a very low flow rate. Then, a thermally-driven moving phase-change micropump was developed in 1995[8], which consisted of only one microchannel and several electrical heaters. The micropump is schematically shown in Fig. 1. Fluid flowing in the microchannel could be pumped in the scanning direction by an electric current cycling through the heaters. Theoretical analyses were developed to describe the pumping mechanism. Ozaki[8] suggested that the large kinematic viscosity difference between the liquid and vapor phases produced the

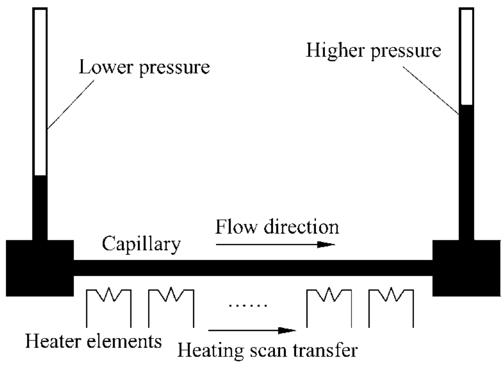

Fig. 1 Structure of thermally-driven phase-change micropump

Received: 2003-05-31; revised: 2004-01-09

∗ Supported by the National Natural Science Foundation of China (No. 59995550-2) and National Key Basic Research and Development (973) Program of China (No. G1999033106)

∗∗ To whom correspondence should be addressed.
E-mail: lizhx@tsinghua.edu.cn; Tel: 86-10-62772919

unidirectional mass flow. Jun and Kim[9] fabricated a much smaller surface-micromachined micropump and found that the two domain pumping forces were vapor pressure and surface tension. DeBar and Liepmann[10] experimentally investigated the micropump and ascribed the pumping principle only to surface tension from the Marangoni effect. Wang and Li[11,12] presented a pressure model to predict the mass flow per cycle, which agreed somewhat with experimental results. They explained that the pumping flow resulted from the instantaneous high pressure during evaporation. All these analyses differed from each other and did not produce satisfactory agreement with experimental results.

This paper presents a theoretical model describing the pumping principle which agrees with experimental results. The analysis shows that the pumping mechanism is mainly due to the large density difference between the liquid and vapor phases and the choking effect of the vapor section.

1 Theoretical Analysis

The dynamic model is based on the heating and cooling conditions shown in Fig. 2. In the model, the heat source moves at a constant speed of U from Point I towards Point O. The fluid in the microchannel is heated and evaporated to create a vapor section (a bubble). Vaporization occurs at Point E while condensation occurs at Point C. The vapor section length, L_C, is a function of both the heating and cooling conditions. The total length of the moving heat source is L_H, and the preheating region where the liquid is heated to boiling L_P in length. Assume dynamic equilibrium between the evaporation and the condensation, and L_C remains constant and the bubble will move with the heat source to pump the liquid in the movement direction.

In general, the fluid flow in the microchannel is laminar due to the very small inner diameter. Therefore, the pressure drops for the three regions in the circular tube are:

$$\Delta p_O = p_E - p_O = \frac{8\mu_L L_O Q_O}{\pi r^4} \quad (1)$$

$$\Delta p_C = p_E - p_C = \frac{8\mu_G L_C Q_C}{\pi r^4} \quad (2)$$

$$\Delta p_I = p_I - p_C = \frac{8\mu_L L_I Q_I}{\pi r^4} \quad (3)$$

where Q denotes the volume flow rates, the subscripts L and G represent liquid and gas, and r is the tube radius.

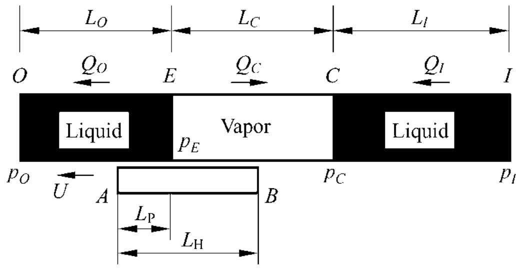

Fig. 2 Dynamic micropump model

Mass conservation equation at the vapor-liquid interface E gives

$$\rho_L Q_O = \pi r^2 U(\rho_L - \rho_G) - \rho_G Q_C \quad (4)$$

while mass conservation equation for the whole tube gives

$$Q_O = Q_I = Q \quad (5)$$

The flow rate can be derived by combining Eq. (1) with Eq. (5):

$$Q = \frac{-F\Delta p + AU(\rho_L - \rho_G)L_C \nu_G}{\rho_L[L\nu_L + L_C(\nu_G - \nu_L)]} \quad (6)$$

where $F = \pi r^4/8$, $A = \pi r^2$, $\Delta p = p_O - p_I$, $L = L_O + L_C + L_I$, ρ is the fluid density, and ν is the fluid viscosity.

Consider a micro liquid element δL moving from A to E. Ignoring the heat dissipation in the liquid section, an energy balance along δL gives

$$\frac{P_H}{L_H} \cdot \delta L \cdot \frac{L_P}{U - \dfrac{Q}{A}} = cA \cdot \delta L \cdot \rho_L \Delta T \quad (7)$$

where P_H is the effective heating power of the entire heater, c is the liquid specific heat, and ΔT is the temperature difference. Therefore, the preheating liquid section length, L_P, is

$$L_P = \frac{cA\rho_L \Delta T\left(U - \dfrac{Q}{A}\right)L_H}{P_H} \quad (8)$$

If the dissipated power per meter in the vapor section is q, an energy balance over the vaporation gives

$$P_H\left(1 - \frac{L_P}{L_H}\right) = q \cdot L_C \quad (9)$$

Combining Eqs. (8) and (9) gives the vapor section length as

$$L_C = \frac{P_H - cA\rho_L \Delta T\left(U - \frac{Q}{A}\right)}{q} \quad (10)$$

The heating condition, embodied by P_H, and the cooling condition, embodied by q, determine the vapor section length, L_C, and indirectly affect the flow rate.

Equations (6) and (10) relate Q and L_C. Qualitative analysis indicated that there is no obvious mass flow if L_C is too long or too short, and an optimal L_C exists for the maximum flow rate.

Equation (6) suggests the essential pumping condition as

$$U > \frac{F\Delta p}{A(\rho_L - \rho_G)L_C \nu_G} \quad (11)$$

Equation (11) shows that unidirectional mass flow occurs only when the heat source moves faster than a critical speed. If the density difference between the liquid and vapor is too small or the vapor kinematic viscosity is not large, the critical speed will be quite high. As a result, the pumping mechanism is mainly due to the large density difference between the liquid and vapor phases and the vapor choking effect. The critical speed is also inversely proportional to the square of the tube diameter, which suggests that this micropump is suitable for micro size applications.

2 Experimental Results

The micropump was tested experimentally to verify its physical principles. The pump characteristics were measured and analyzed, including pumping pressure and flow rates for different heating and cooling conditions[13].

The experimental system is shown in Fig. 3. The working fluid was distilled water. A stainless steel microtube was used as the pump body with DC currents to heat the tube. The dimensions and the number of subsections of the microtubes used in the experiments are listed in Table 1.

First, the flow rates were measured for different heating conditions using Tube 1. The results are shown in Figs. 4 and 5, in which the switch time, t_s, is the time for heating one subsection per cycle. The two figures indicate that an optimal combination of heating current and switch time results in the maximum flow rate.

Table 1 Dimensions and divisions of the two micro tubes used in the experiments

	Inner diameter (μm)	Outer diameter (μm)	$\frac{L}{\text{cm}}$	Number of subsections	$\frac{\Delta L}{\text{cm}}$
Tube 1	200	300	30	5	4
Tube 2	300	400	30	6	3.5

Note: ΔL is the subsection length.

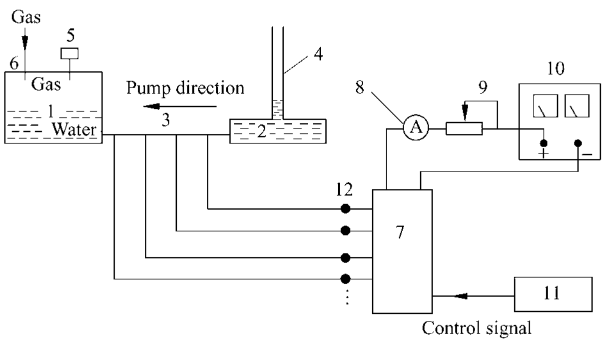

Fig. 3 Experimental system

1, High pressure vessel; 2, Lower pressure vessel; 3, Stainless steel capillary; 4, Glass tube with scale; 5, Micro pressure sensor; 6, Valve; 7, Heating controller; 8, Amp meter; 10, Resistor; 10, Power supply; 11, Computer; 12, Indicator lights

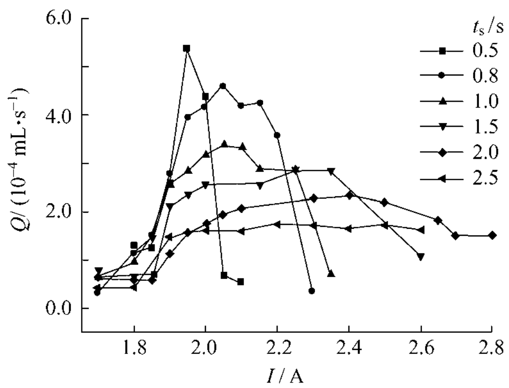

Fig. 4 Flow rate vs. heating current *I* of Tube 1 for given switch time

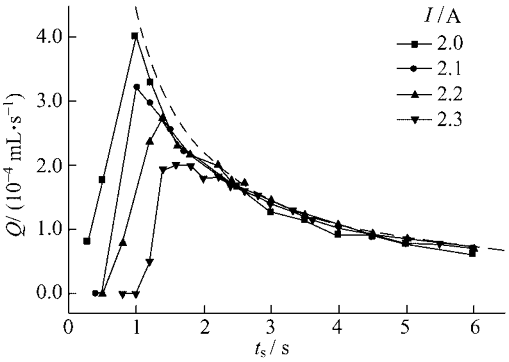

Fig. 5 Flow rate vs. switch time of Tube 1 for given heating currents. The dashed line is an inverse proportion function curve.

The measured flow vs. pressure characteristics for Tube 1 are shown in Fig. 6. The maximum flow rate nearly reached 5.0×10^{-4} mL • s^{-1} and the maximum pump pressure was over 20 kPa.

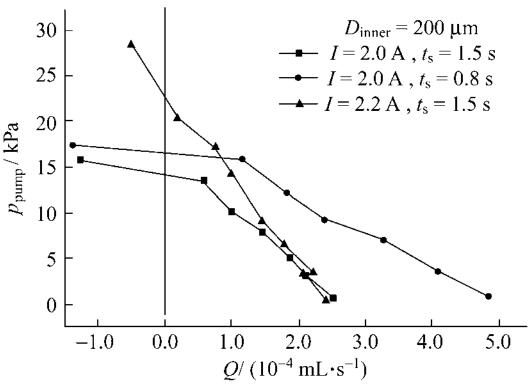

Fig. 6 Flow rate vs. pumping pressure characteristics for Tube 1

The effect of different cooling conditions on the pumping characteristics was studied experimentally using natural and forced convective cooling of Tube 2. A fan was used to form the forced convection cooling. The pumping flow rate variation for varying heating current is shown in Fig. 7.

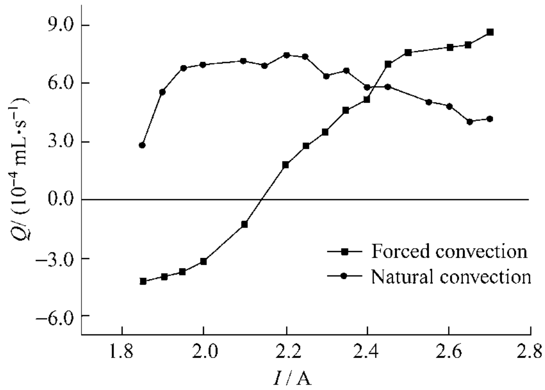

Fig. 7 Flow rate variations for different cooling conditions using Tube 2 and a switch time of 2 s

3 Numerical Simulations

The theoretical equations were solved numerically to compare with the experimental results. Since the moving constant-length bubble was assumed to always exist in the tube in the theoretical model, and must be created at the beginning of a cycle in the experiments, the real averaged flow rate was modified to be

$$Q^* = Q\cdot(1-\frac{L_C}{L}) \tag{12}$$

Equations (6), (10), and (12) were solved numerically with the parameters obtained from the experiments. The properties and parameters are listed in Table 2.

Table 2 Properties and parameters used in the simulations

$\frac{L}{\text{m}}$	$\frac{\Delta L}{\text{cm}}$	$\frac{\rho_{\text{L}}}{\text{kg•m}^{-3}}$	$\frac{c_{p\text{L}}}{\text{kJ•kg}^{-1}\text{•℃}^{-1}}$	$\frac{T_A}{℃}$	$\frac{T_E}{℃}$	$\frac{V_{\text{G}}}{\text{m}^2\text{•s}^{-1}}$	$\frac{V_{\text{L}}}{\text{m}^2\text{•s}^{-1}}$
0.3	4.0	1×10^3	4.18	60	100	20.12×10^{-6}	0.3×10^{-6}

The heat source velocity is $U=\dfrac{\Delta L}{t_{\text{s}}}$.

For a microtube cooled by natural convection and radiation, together with the longitudinal conductive heat loss, the calculated heat loss per meter in the vapor section was q=7.5 W/m.

Analysis of the effective heating power showed that as the fluid vaporized, the heat transfer coefficient decreased and the effective heating power decreased. Therefore, the effective heating power was described by

$$P_{\text{H}} = I^2 R\cdot \text{e}^{-t_{\text{s}}} \tag{13}$$

where I is the heating current and R is the electrical resistance of the heated section.

Figures 8-10 show the simulated flow versus pressure characteristics corresponding to the experimental data using the parameters of Tube 1. Figure 11 shows the results for Tube 2 with different cooling conditions, in which the forced cooling heat transfer per meter was assumed to be 50 W/m. The numerical results compare well with the experimental data.

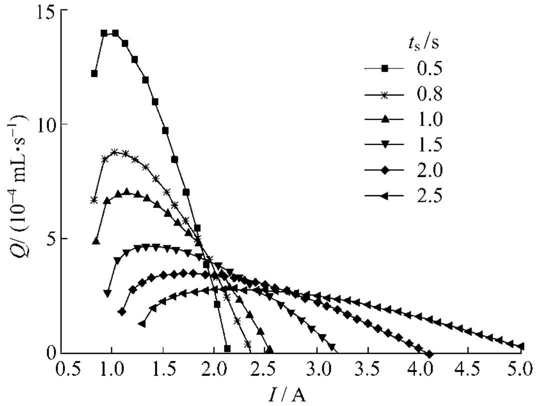

Fig. 8 Simulated flow rate variations in Tube 1 for different switch times

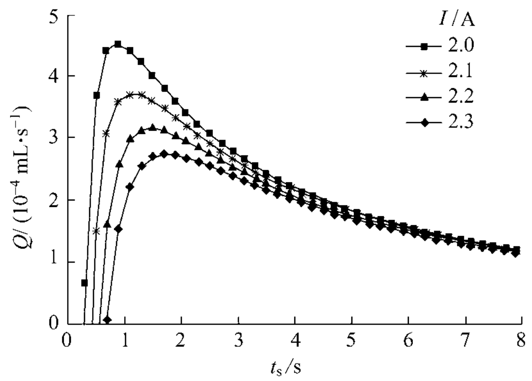

Fig. 9 Simulated flow rate variations in Tube 1 for different heating currents

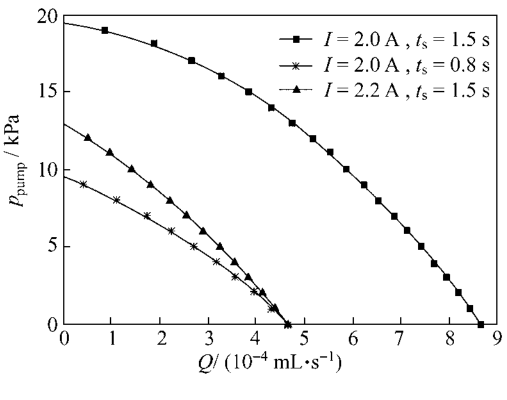

Fig. 10 Simulated flow rate vs. pumping pressure characteristics for Tube 1

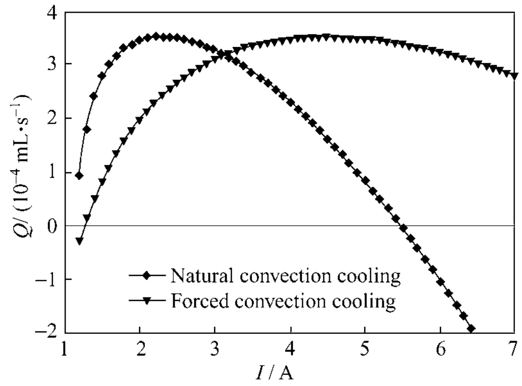

Fig. 11 Simulated flow rates in Tube 2 for different cooling conditions with a switch time of 2 s. Natural cooling heat loss per meter was 7.5 W/m and forced cooling heat loss per meter was 50 W/m.

4 Conclusions

Experiments with different diameter micropumps were performed for different heating and cooling conditions. For a 200-μm diameter micropump, the maximum flow rate reached 33 μL/min and the maximum pump pressure was over 20 kPa. The theoretical results agree well with the experimental data, which shows that the model accurately describes the physics. Both the experimental and simulation results show that there are optimal heating and cooling conditions for the maximum flow rate.

References

[1] Wang Moran, Li Zhixin. Investigation process of micropump based on MEMS. *Journal of Transducer Technology*, 2002, **21:** 59-61. (in Chinese)

[2] Darabi J, Ohadi M M, DeVoe D. An electrohydrodynamic polarization micropump for electronic cooling. *Journal of Microelectromechanical Systems*, 2001, **10**: 98-106.

[3] Jang J, Lee S S. Theoretical and experimental study of MHD (magnetohydrodynamic) micropump. *Sensors and Actuators*, 2000, A**80**: 84-89.

[4] Yuan H, Prosperetti A. The pumping effect of growing and collapsing bubbles in a tube. *Journal of Micromechanics & Microengineering*, 1999, **l9**: 402-413.

[5] Tsai J H, Lin L. A thermal bubble actuated micro nozzle-diffuser pump. In: Technical Digest. MEMS 2001, 14th IEEE International Conference on Micro Electro Mechanical Systems, 2001: 409-412.

[6] Lin L. Microscale thermal bubble formation: Thermophysical phenomena and applications. *Microscale Thermophysical*

Engineering, 1998, **12**: 71-85.

[7] Mizoguchi H, Ando M, Mizuno T, et al. Design and fabrication of light driven micropump. In: Proc. IEEE Micro Electro Mechanical Systems: An Investigation of Micro Structures, Sensors, Actuators, Machines and Robots. Travemunde, Germany, 1992: 31-36.

[8] Ozaki K. Pumping mechanism using periodic phase changes of a fluid. In: Proceedings IEEE Micro Electro Mechanical Systems Conference. New York, 1995: 31-36.

[9] Jun K T, Kim C J. Microscale Pumping with Traversing Bubbles in Microchannels. In: Technical Digest. Solid-State Sensor and Actuator Workshop. Transducer, Cleveland Heights OH, USA, 1996: 144-147.

[10] DeBar M J, Liepmann D. Fabrication and performance testing of a steady thermocapillary pump with no moving parts. In: Proceeding of IEEE MEMS-2002 Conference. San Diego, USA, 2002: 109-112.

[11] Wang Moran, Li Zhixin. Pressure model of phase-change micropump. In: Proc 10th National Academic Conference on Engineering Thermalphysics of China. Qingdao, 2001: 240-244. (in Chinese)

[12] Wang Moran, Li Zhixin, Chen Zejing. The pumping effect of phase transition in a micro tube. *International Journal of Nonlinear Sciences and Numerical Simulation*, 2002, **3**: 565-568.

[13] Li Zhixin, Wang Moran, Tan Liyan. Experimental investigation on phase transformation type micropump. *Chinese Science Bulletin*, 2002, **47**: 518-522.

(Continued from page 687)

4 Conclusions

Expressions for the energetic coefficient of restitution are given considering various slip contact modes based on the model of local elastic-plastic planar rigid-body collisions with friction. The analysis has shown that a method to obtain the coefficient of restitution for oblique collisions has been given, which can provide a theoretical guide for experiments on collisions.

It can also be noted that the results in this paper only apply for low-speed collisions and preserve the traditional assumptions for such calculations. The precision of the model depends on the precision in the model for the normal and tangential contact forces.

References

[1] Stronge W J. Rigid body collisions with friction. *Proc. Roy. Soc. Lond.*, 1990, **A431**: 169-181.

[2] Thornton C. Coefficient of restitution for collinear collision of elastic spheres. *ASME J. of Applied Mechanics*, 1997, **64**: 383-386.

[3] Xiang Zhang, Voc Vu-Quoc. Modeling the dependence of the coefficient of restitution on the impact velocity in elasto-plastic collisions. *International Journal of Impact Engineering*, 2002, **27**: 317-341.

[4] Adams G G, Tran D N. The coefficient of restitution for a planar two-body eccentric impact. *ASME J. of Applied Mechanics*, 1993, **60**: 1058-1060.

[5] Chang W R, Ling F F. Normal impact model of rough surfaces. *ASME Journal of Tribology*, 1992, **114**: 439-447.

[6] Stronge W J. Impact Mechanics. London: Cambridge University Press, 2000: 35-59.

[7] Gilardi G, Sharf I. Literature survey of contact dynamics modeling. *Mechanism and Machine Theory*, 2002, **37**: 1213-1239.

[8] Nobre J P, Dias A M, Gras R. A study on elasto-plastic impact friction. *Wear*, 1999, **230**: 133-145.

[9] Stronge W J. Generalized impulse and momentum applied to multibody impact with friction. *Mechanics of Structures and Machines*, 2001, **29**: 239-260.

[10] Brogliato. Nonsmooth Mechnics. London: Springer, 1999: 105-171.